SITE TESTING AT OBSERVATORIO ASTRONÓMICO NACIONAL IN SAN PEDRO MÁRTIR

J. Echevarría, M. Tapia, R. Costero, L. Salas, Rm. Michel,
Rl. Michel, M. A. Rojas, R. Muñoz, J. Valdez, J. L. Ochoa,
J. Palomares, and O. Harris

Instituto de Astronomía
Universidad Nacional Autónoma de México

R. H. Cromwell and N. J. Woolf

Steward Observatory, University of Arizona

and

S. E. Persson and D. M. Carr

The Observatories of the Carnegie Institution of Washington

RESUMEN

Se han realizado mediciones detalladas sobre la turbulencia atmosférica y las condiciones climatológicas en el sitio del Observatorio Astronómico Nacional en San Pedro Mártir. Los resultados obtenidos durante tres años con el Telescopio de Pruebas de Sitio del Observatorio de Steward, arrojan una *calidad de imagen* cuya mediana es de 0.61 segundos de arco y con un primer cuartil de 0.50 segundos de arco. Estos valores se confirman con mediciones independientes y simultáneas realizadas con el monitor de los Observatorios de Carnegie. Se detecta una variación en función de la época del año, con mejores valores durante la primavera y el verano, con una mediana de 0.59 segundos de arco, comparado con 0.69 segundos de arco para el otoño y el invierno. Las mediciones con el Arreglo Micro Térmico muestran que la *calidad de imagen* disminuye 0.1 segundos de arco a 15 metros de altura. La *calidad de imagen* pareciera no depender fuertemente de las variables meteorológicas como velocidad y dirección del viento, humedad, o temperatura externa.

ABSTRACT

Detailed measurements of the atmospheric turbulence and climatological conditions have been carried out at the site of the Observatorio Astronómico Nacional at San Pedro Mártir. The results obtained during a three year period with the Site Testing Telescope from Steward Observatory yielded a median *seeing* of 0.61 arcsec and a first quartile of 0.50 arcsec. These were confirmed by independent and simultaneous measurements with the monitor of the Observatories of the Carnegie Institution. We detect a seasonal dependence on the *seeing*, with better results during spring and summer when we find a median of 0.59 arcsec, compared with autumn and winter, which have a median of 0.69 arcsec. Measurements with the Micro-Thermal Array show that the *seeing* decreases by 0.1 arcsec at a height of 15 meters. The *seeing* does not seem to depend strongly on meteorological variables like wind direction and velocity, humidity or external temperature.

1. INTRODUCTION

In the late sixties, the Instituto de Astronomía of the Universidad Nacional Autónoma de México searched for a new observatory site, since the Observatorio Astronómico Nacional, first at Tacubaya, México City and later at Tonantzintla, Puebla, was already inside densely populated areas and therefore, highly contaminated. Through satellite photographs it was found that the northern part of Baja California was one of the three best cloud-free areas in the world. After several meteorological studies, the Observatorio Astronómico Nacional was established at the Sierra of San Pedro Mártir (SPM).

It lies within the NE part of the San Pedro Mártir National Park, and it is at the top of a spur arising from the San Felipe desert. At present, it has three telescopes of diameters 0.84-m, 1.5-m and 2.1-m (see e.g., Moreno-Corral, Costero, & Schuster 1994).

A number of studies on the climatological properties of this site have been reported, mainly during the first years of operation of SPM (Mendoza 1971, 1973; Mendoza, Luna, & Gómez 1972; Walker 1971, 1984; Alvarez 1982, Alvarez & Maisterrena 1977; Tapia 1992). The sky emission at 10 μm has been reported by Westphal (1974), and the atmospheric opacity at 215 GHz has been discussed by Hiriart et al. (1997).

The value and possible uses of a terrestrial site depend on the site characteristics. Modern astronomy requires a site with low water vapor and good image sharpness at the height to which a telescope can be built. Therefore, a coordinated campaign in collaboration with the Steward Observatory and the Carnegie Institution started early in 1992 to evaluate the atmospheric turbulence and climatological conditions in SPM. In this paper we present the results of three years of collaborative efforts.

Fig. 2. The *Low xy* sample ($|x-y| < 0.2$ arcsec) separated by their independent x and y measurements.
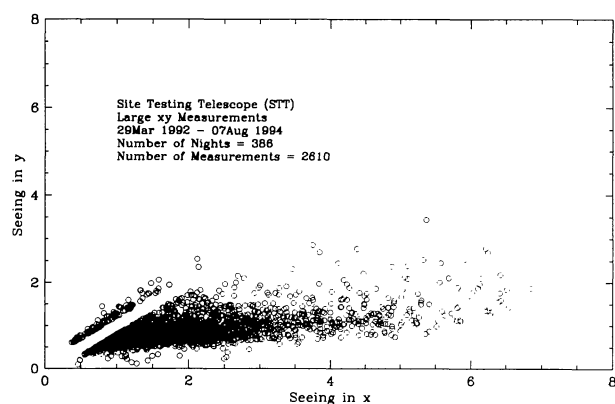
Fig. 3. The *High xy* sample ($|x - y| > 0.2$ arcsec) separated by their independent x and y measurements.
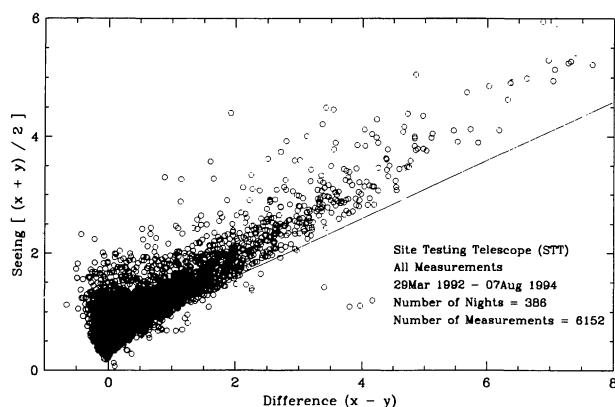

Fig. 1. The total *seeing* $(x + y)/2$ as a function of the difference $(x - y)$ which shows the effect of the wind in the telescope structure, and hence on the *seeing* measurements.
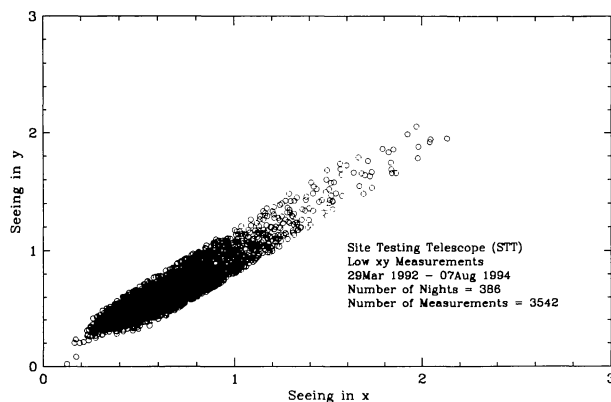
2. ATMOSPHERIC TURBULENCE AND TEST INSTRUMENTS

Stellar images recorded by large telescopes are much bigger than the diffraction limit as they are severely degraded by thermal effects in the dome, the building itself, and the immediate surroundings. The image size also depends on the local atmospheric turbulence which, in turn, depends on the geographical layout of the site and on turbulence in the upper atmosphere. The overall quality of the optical image, as degraded by thermal inhomogeneities in the lightpath is known as *seeing*. A proper definition of this parameter will be given in the next section.

We have measured the *seeing*, during a period of three years, at a site located a few hundred meters to the west of the existing telescopes at SPM. This site is located at 31°02′44″ N, and 115°28′09″ W, at an altitude of 2800 m above sea level (Alvarez & Moreno 1995). In this location, the NE winds tend to
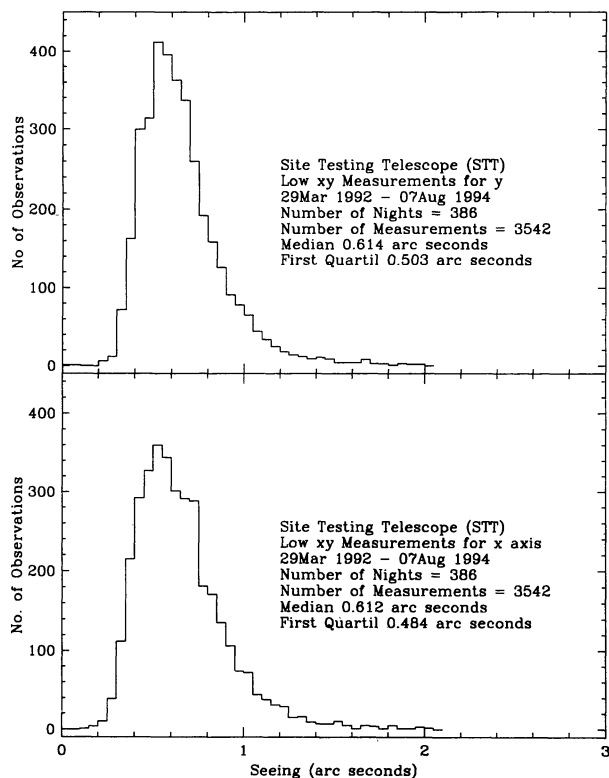
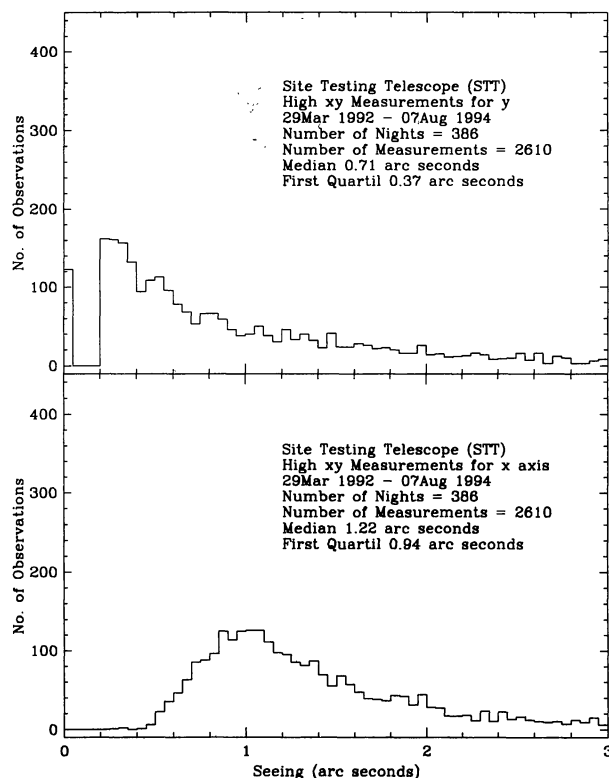Fig. 4. The *seeing* distribution for the independent x and y measurements in the *Low xy* sample.

Fig. 5. The *seeing* distribution for the independent x and y measurements in the *High xy* sample.

follow a long and wide valley which runs between the observatory and the northern Venado Blanco peak, while the SW winds blow directly on the site after climbing a smooth slope.

The results reported here were obtained with three different systems. The first one is the Site Testing Telescope from Steward Observatory; designed to observe Polaris. The second one is the Carnegie Monitor which can observe and track any star. And the third one is the Micro-Thermal Array which consists of a series of platinuum detectors to measure temperature differences located at different heights.

2.1. *The Site Testing Telescope*

The Site Testing Telescope (STT) in use at SPM is one of the two telescopes employed by Cromwell, Haemmerle, & Woolf (1988) and Cromwell, Blair, & Woolf (1998) for site testing at Mount Graham, Arizona. It consists of a 31.75-cm f/4 Cassegrain primary mirror followed by an f/15 secondary and a microscope objective focal expander that gives a final focal ratio of f/99. The telescope is mounted on an open guy-wired quadrapode tube structure at a height of 3.8 m above ground without enclosure. A Sanyo CCD camera, which employs a frame transfer

method of interlacing two TV fields each with an exposure time of 1/60 s, was attached to the Cassegrain focus and a video signal in VHS format was recorded for about 90 s at a speed of 30 frames per second (selecting one of the two interlaced frames). Further details can be found in Cromwell et al. (1988). The VHS images are later reduced using a computer-controlled frame grabber. Since no tracking is done, the image of Polaris moves in practically a straight line along the CCD video. The size of the stellar image is therefore, measured as the standard deviation of the motion of the star within about 2700 frames. Two independent orthogonal measurements are made in every run, one in azimuth and one in altitude, corresponding to the x and y axis, respectively. Further discussion will be given in § 3.1.

2.2. *The Micro-Thermal Array*

The Micro-Temperature Array (MTA), is a high precision instrument designed to obtain accurate measurements of minute variations in air temperature. The system is that used to measure several sites in the Mt. Graham Astrophysical Area and at the site for the Multiple Mirror Telescope at Mt. Hopkins, Arizona (Cromwell et al. 1992, 1998). It
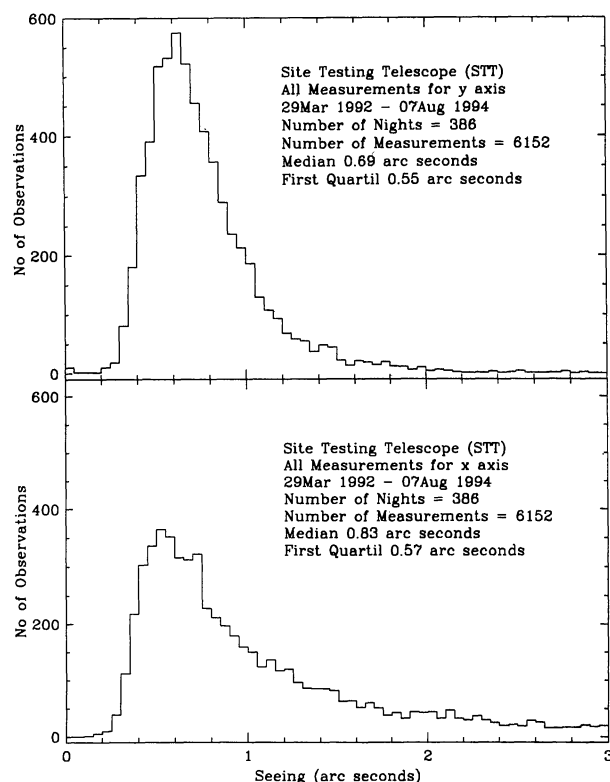
Fig. 6. The *seeing* distribution in the x and y axis for all observations.
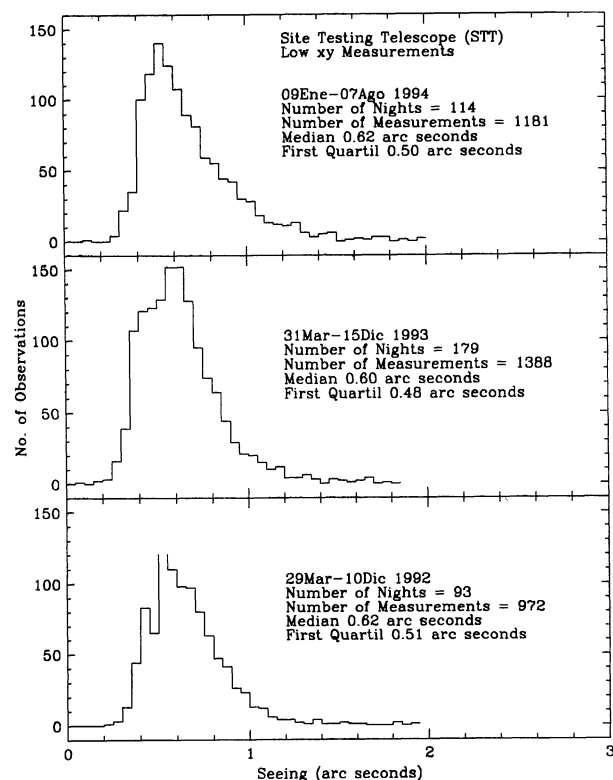

Fig. 7. *Seeing* values (*Low xy* Measurements) with the STT (see § 3.1) for individual years.

basically consists of a telescoping 30 m aluminium mast, five pairs of platinum-wire temperature difference sensors, and a portable computer equipped with a multi-channel A/D (analog-to-digital) converter unit.

The actual array part of the instrument is comprised of the five temperature difference sensors, which are wired into a multi-conductor cable at 5 m intervals. Each sensor pair consists of two platinum-wire sensor units separated by 1 m and a differential amplifier housed in a center enclosure. At dusk or shortly after, the array is hoisted into position using a pulley line which is looped through a top cross-arm on the tower. The portable computer records the temperature differences detected by each sensor pair during the night, storing the data on a floppy diskette for later analysis. At dawn the array is lowered from the tower and enclosed in a small plastic cooler chest during the day.

We define the coefficient C_T^2 as the square of the temperature difference of each sensor pair. This coefficient is related to the local optical turbulence at each measured height above the ground (e.g., Woolf 1982). The local values are integrated to the median value at 100 m which does not depend on the local site conditions but on the turbulence of the free at-
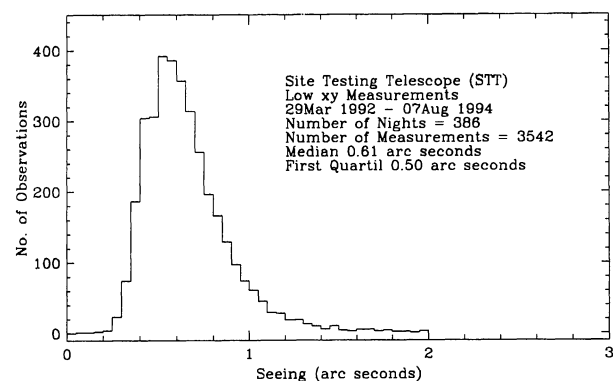

Fig. 8. The total *seeing* distribution measured with the STT for the three years of the campaign.

mosphere (see Cromwell et al. 1998). The local turbulence is a consequence of the inhomogeneous mixing of hot air cells with cells cooled by the ground and by the interaction of the wind with the local orography.

Carnegie Monitor
3 Sept. 1992 – 10 Aug. 1993
Number of Nights = 99
Median 0.63 arc seconds
First Quartil 0.48 arc seconds

Carnegie Monitor
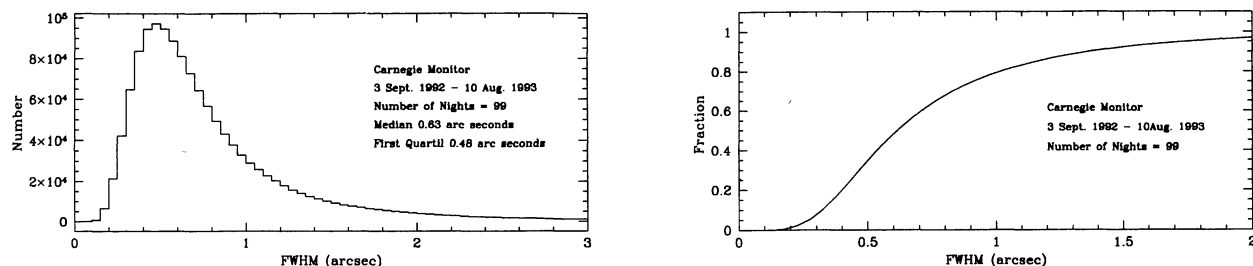3 Sept. 1992 – 10Aug. 1993
Number of Nights = 99

Fig. 9. Left panel: Distribution histogram of the FWHM size of the *seeing* disk as measured with the CM. Right panel: Fraction of the time that the FWHM *seeing* is better than indicated.

22 May

22 May
med. = 0.43

25 April

25 April
med. = 0.58

22 April

22 April
med. = 1.12

24 June

24 June

FWHM (arcsec)
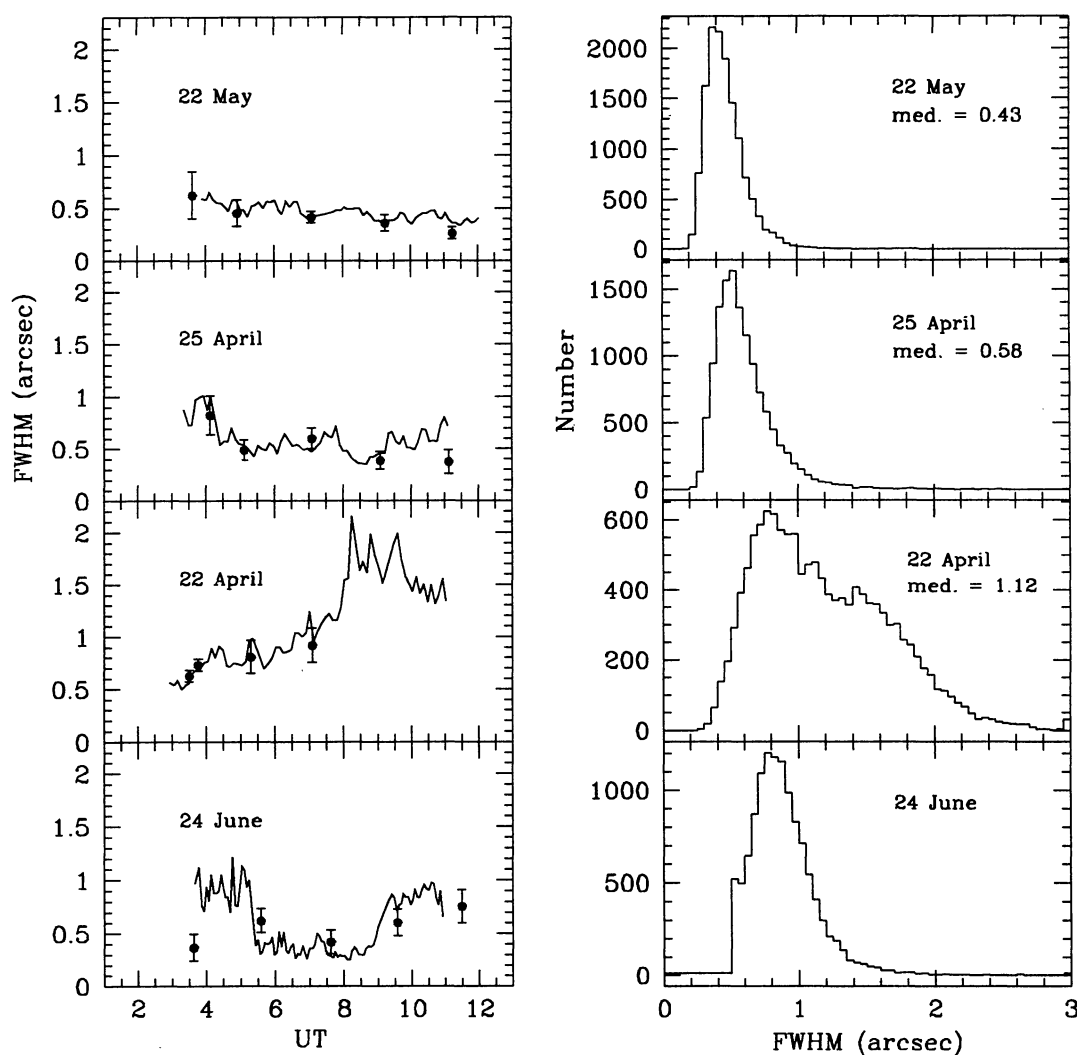
UT

Number

FWHM (arcsec)

Fig. 10. Behaviour of the size (FWHM) of the *seeing* disk during three typical nights of good (22 May), medium (25 April) and bad (22 April) *seeing* and also one (24 June) of the several nights which had to be discarded because of wind shaking of the telescope. In the left panel the FWHM of the stellar image along the four nights are ploted. Continuous lines are from the CM and the points with error bars are mean and scatter of several measurements with the STT. The right panel shows the respective histogram from the CM for each night.
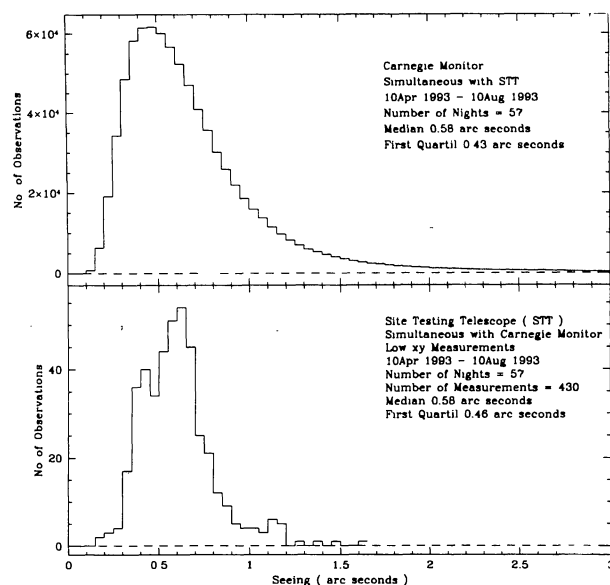
Fig. 11. *Seeing* distribution for the nights when the CM and the STT were gathering data simultaneously.

2.3. *The Carnegie System*

The seeing-measuring system, thereafter called the Carnegie Monitor (CM) is described in detail by Persson, Carr, & Jacobs (1990). It consists of a Questar 20-cm Maksutov telescope on an equatorial mount with drive motors. The data acquisition, telescope control and on-line data reduction are done by a dedicated PC computer storing the statistics of the measurements every ten minutes on disk. The principle of operation is to measure the position of a stellar image by rapidly shifting it between two detectors, in such a way that a perfectly centered image would spend exactly half its time on each detector. The difference in time spent on the two detectors is linearly proportional to the displacement from the central position. Based on this principle, the system measures the size of the image caused by its motion at frequencies between 2 and 200 Hz. In this way, the exposure time is 5 msec. Persson et al. (1990) describes the calibration and data reduction methods to yield the predicted FWHM of the size of the image for a large telescope at one air mass in yellow light. A *seeing* comparison campaign between Las Campanas Observatory and Cerro Vizcachas was conducted by Sarazin (1990). This intercomparison included simultaneous observations with a Differential Image Motion Monitor (DIMM) and the CM. Although the purpose of this work was not to analyse the accuracy of the CM, the results are that, discarding high wind speed conditions (to avoid measurements on a non differential mode system), the CM and the close

by DIMM measurements are rather well correlated, although the first gives a *seeing* value in average 20 percent better. As discussed by Sarazin, this is not due to a calibration effect, but rather depends on the type of turbulence and its temporal characteristics, since the DIMM monitor was closer to the ground (at 2 m) than the CM (at 5 m).

The whole system was received on loan from The Observatories of the Carnegie Institution and installed in SPM in August 1992 and remained in operation till late 1993. It was mounted on an 8 meter-high concrete pedestal unconnected to the outer cylindrical metal shield and retractable dome. The telescope, dome and on-line drive, data acquisition and reduction computer programs were the same as those used for monitoring the *seeing* in Las Campanas and Cerro Pachon, Chile. For technical operational reasons, data were gathered only during the months of September 1992 and April to August 1993. The telescope tracks and auto-guides a bright star for several hours and the dome consists of two hemispheres to protect the telescope from the wind which can severely affect the measurements by causing random vibrations to the telescope. Unfortunately, in a small fraction of nights, the operator did not consider the wind direction when selecting the stars, and thus, bad positioning of the dome resulted in telescope shaking. During these nights, the measurements showed extremely different values for each star observed throughout the night, depending on how strong the wind shook the telescope at each star (and dome) position. These nights had to be discarded altogether.
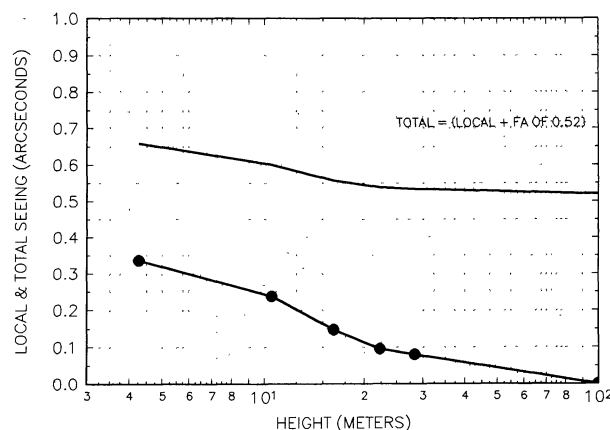

Fig. 12. MTA observations during the first months of STT measurements. The filled circles are the local *seeing* values derived from the C_T^2 values at each altitude. The upper curve represents the total *seeing*, using a *free atmosphere seeing* of 0.52 arcsec.
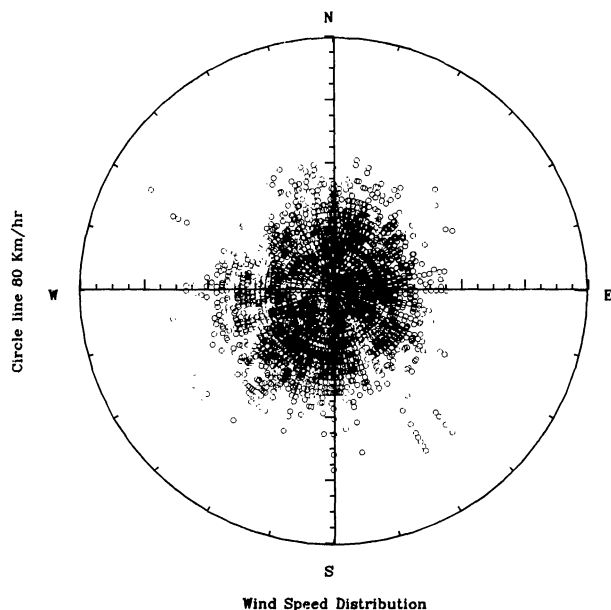
Wind Speed Distribution

Fig. 13. The wind speed distribution. Nearly 6150 observations covering 386 nights are plotted independently of the *Low xy* and *High xy* selection criteria (see text).

2.4. *The Meteorological Station*

The meteorological station is a Weather Monitor II system from Davis Instruments. It measures wind speed and its direction, as well as external temperature and humidity. This station is located at the peak of the MTA tower and has an interface via an RS-232 port with a PC computer. The data is stored in the hard disk and visual readings are also taken simultaneously with the STT and MTA measurements.

3. SEEING RESULTS

3.1. *Site Testing Telescope Measurements*

Seeing measurements with the STT were obtained during 3 years spanning from March 29, 1992 to August 7, 1994, over a total of 386 nights summing 6152 observations.

Since no dome or any other kind of protection against the environment covers the telescope, its structure has been designed mechanically to provide a very stable platform. A systematic error in securing the telescope mounting to the ground during the SPM tests produced extreme stiffness in the NS (y axis) direction so that the image oscillates with the
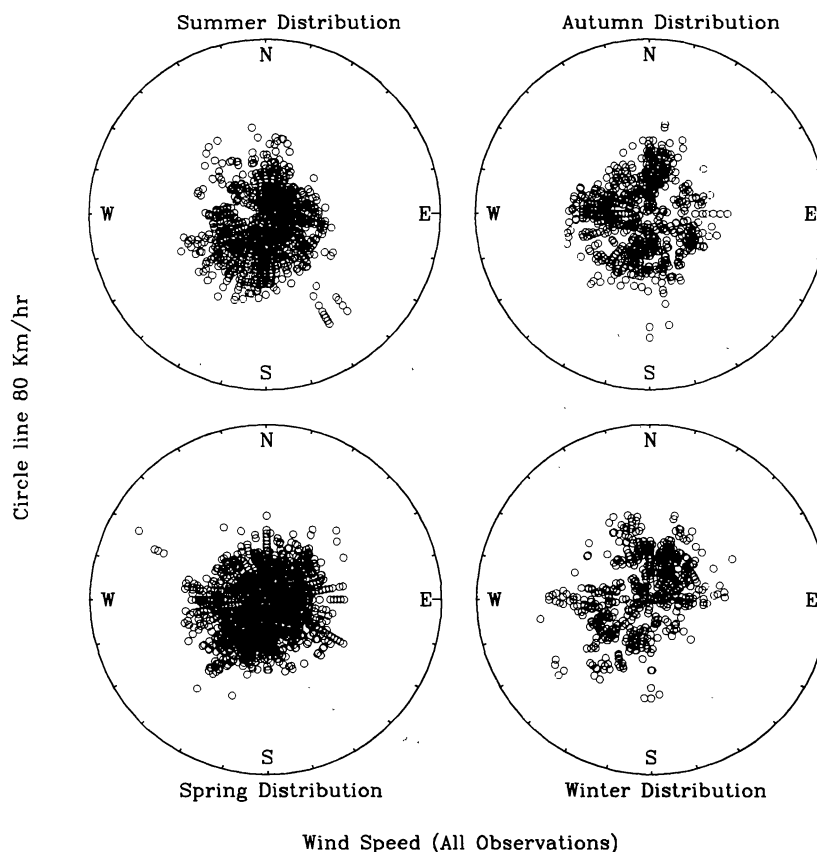

Wind Speed (All Observations)

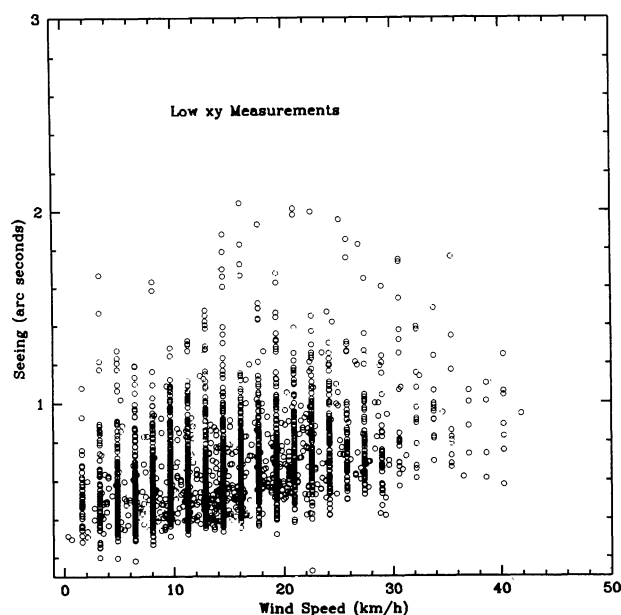Fig. 14. Wind speed distribution as a function of season.

Fig. 15. *Seeing* as a function of wind speed for *Low xy* measurements. No correlation is seen, except for a lack of low *seeing* data for high wind speed.

wind mainly in the EW direction (x axis). Therefore, it is easy to deconvolve the motion of the stellar image of Polaris due to the atmospheric turbulence from wind oscillations when present. The oscillations due to the wind are seen in these video images as abrupt zig-zag displacements of Polaris in the EW direction. During the reduction process the observations were tagged by visual inspection as *Trusted* Observations or *Untrusted* Observations. Figure 1 shows the effect of the wind in the *seeing* measurements where we have plotted the difference $(x - y)$ against the total *seeing* $(x + y)/2$. It is evident from this graph that there is a standard distribution for $|x-y| < 0.2$ while for values greater than 0.2 the wind makes an appreciable effect. If we assume that no wind oscillation is present in the y axis, then it is easy to show that $(x+y)/2 = S + (x - y)/2$, where S is the real *seeing*. This relation is shown in Figure 1 as a solid line. It is reasonable to assume that some wind oscillation effect is present in the altitude axis as no structure is perfectly rigid in one axis and flexible in the other, but this quantity in unknown. The fact that most observations with $x - y > 0.2$ arcsec are above this line is an indication that such wind oscillations are present in the y axis. It is possible to correct the
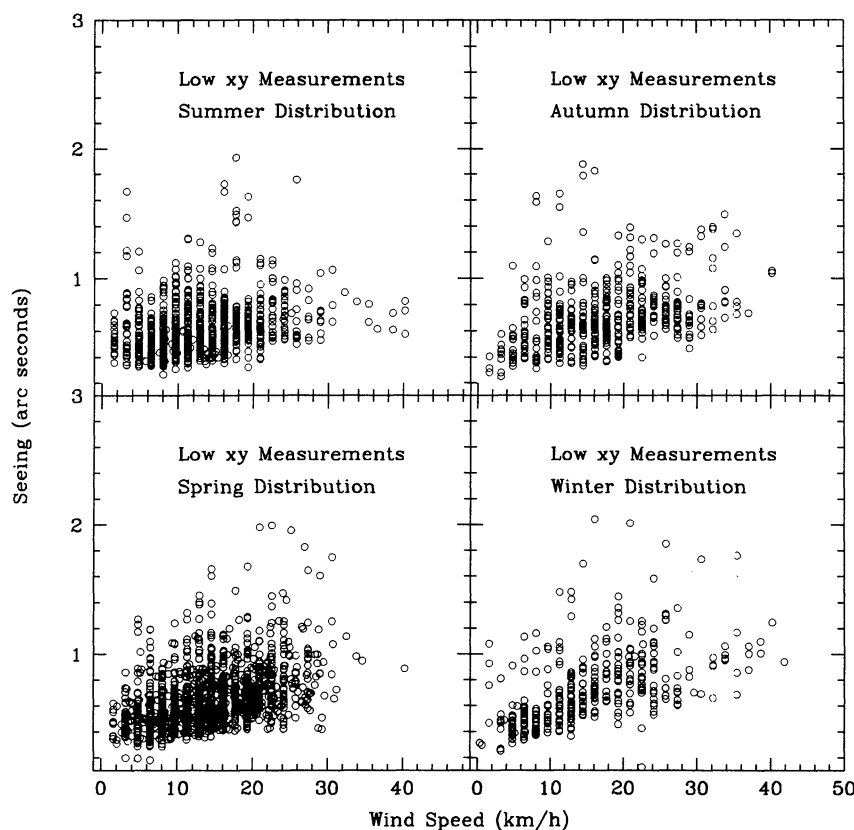

Fig. 16. *Seeing* versus wind speed as a function of season. In this case the slight correlation observed in Fig. 15 is not clearly present during spring and summer, but it is indeed present during autumn and winter.
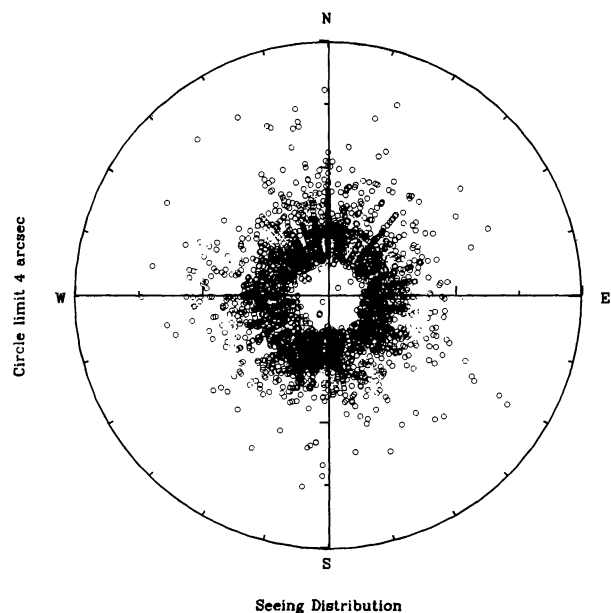
data affected by the wind assuming no effect in the y direction and obtain an upper limit to the median *seeing*, by using the above equation. We have not attempted to make such a correction, but instead, we have analysed both axis independently. We have separated the entire sample in two groups: those with $|x - y| < 0.2$ arcsec, (hereinafter called *Low xy*) and those with $|x - y| > 0.2$ arcsec, (hereinafter called *High xy*). This provides a more quantitative criteria than the *Trusted* and *Untrusted* data defined during the reduction.

Figure 2 shows the *Low xy* data. The values obtained in both axis are similar, with a slope equals unity. We compare this with the *High xy* data, depicted in Figure 3, which has a large range in x values, while the y values remain low. The *seeing* distribution for both axis are shown in Figure 4 and Figure 5 for the two samples. In the case of the *Low xy* data the distributions are very similar, with a median value around 0.61 arcsec; while in the case of *High xy* data the medians are not only very different (1.22 arcsec for the x axis and 0.71 arcsec for the y axis), but their distributions are not the expected ones from atmospheric turbulence.

Seeing Distribution

Fig. 17. *Seeing* as a function of wind direction for *Low xy* measurements.

Summer Distribution   Autumn Distribution

Circle limit 4 arcsec

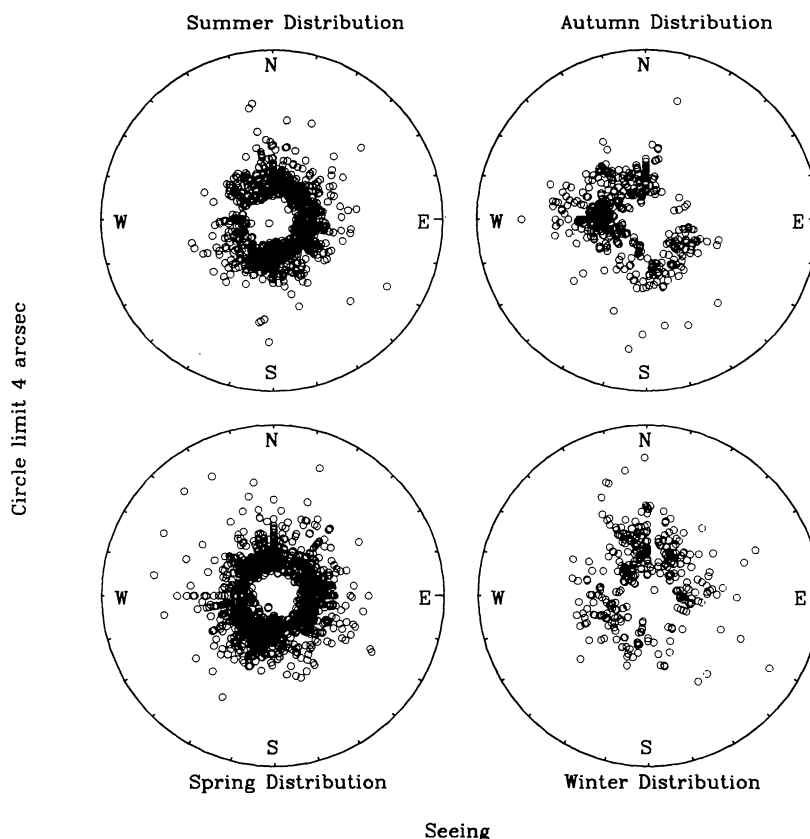Spring Distribution   Winter Distribution

Seeing

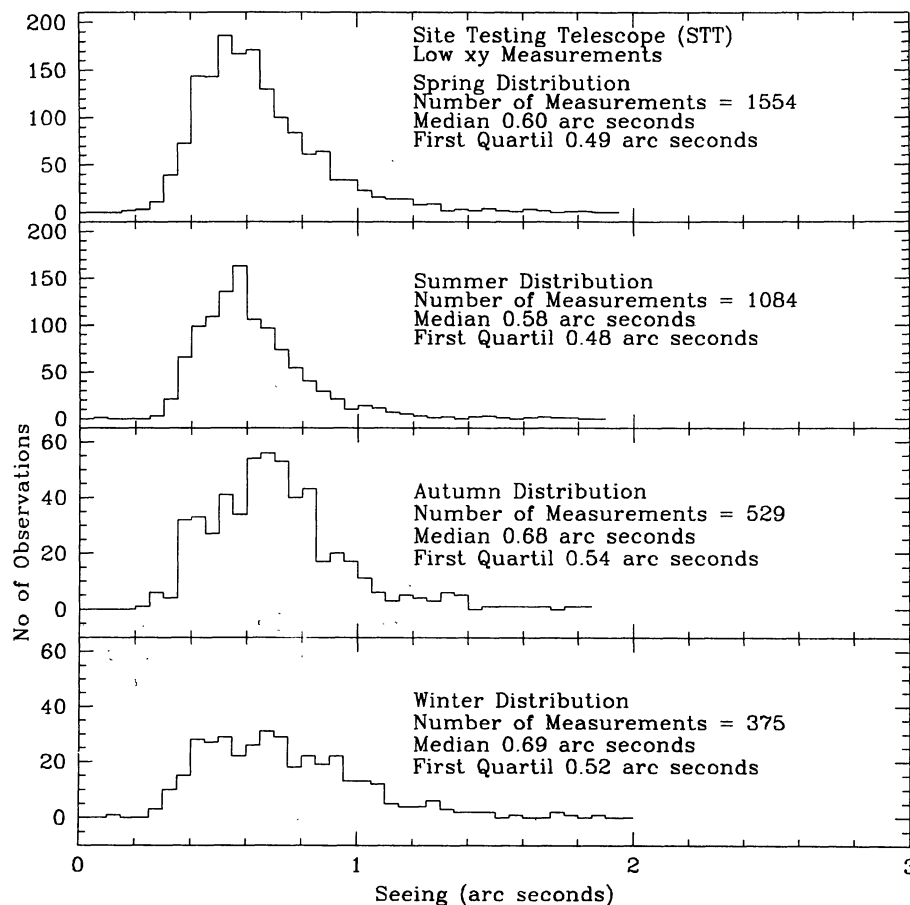Fig. 18. *Seeing* versus wind direction as a function of season.

Fig. 19. *Seeing* distribution as a function of season.

The *seeing* distributions for both axis, including both the *Low xy* and *High xy* sample, are shown in Figure 6. Clearly the *x* data for the *High xy* sample should not be trusted and caution should be taken if we include the *y* data.

The *Low xy* measurements are shown in Figure 7 for individual years and in Figure 8 for the overall data. The distributions are roughly equal, although there is a larger upper tail in 1994. The median values are very similar. The total *seeing* distribution, shown in Figure 8, has a median of 0.61 arcsec and a first quartil of 0.50 arcsec.

3.2. *Carnegie Monitor Measurements*

Seeing measurements have been obtained with the CM for a total of 114 nights, from September 3, 1992 to August 10, 1993. Figure 9 shows the histogram, distribution and statistics of all 99 nights for which we have reliable data, excluding 15 clearly affected by wind shaking the telescope (see below). Not plotted are the data with $\theta > 3$ arcsec, but these were included in the statistics. The median value for the 99 nights is 0.63 arcsec, with a first quartil of 0.48 arcsec.

Figure 10 shows the behaviour of the FWHM size of the *seeing* disk during three typical nights of good (22 May), medium (25 April) and bad (22 April) *seeing*. The value of the FWHM *seeing* averaged over 10 minute intervals along each night and the histogram of all individual measurements are shown as continuum lines. Also shown is the night of June 24, one of the several nights which had to be omitted in this study because of wind shaking the telescope as explained in § 2.3. During this troubled night, four different stars were observed. The drop and increase in the value of the *seeing* at UT 5:15 and 9:15 UT, respectively, coincide with star changes. Clearly the first and last stars were observed with the telescope in a position where the dome did not protect it properly.

3.3. *Simultaneous STT and CM Measurements*

In spite of the fact that the STT and CM data represent totally independent observations, and were reduced following different methods, the agreement between the two sets is quite remarkable.

During single nights, no significant differences were found between each system and this is illus-
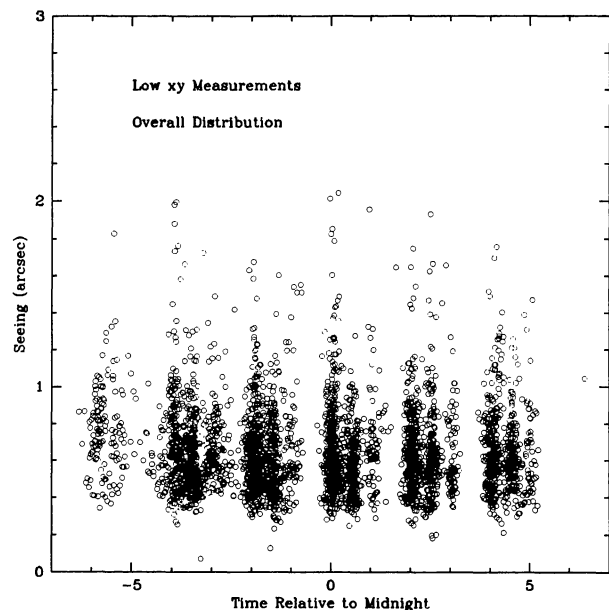
Fig. 20. *Seeing* as a function of time with with respect to midnight.

trated in the left hand panels of Figure 10 for the four sample nights. Here, the points and error bars represent the average and scatter values of 3–5 individual STT measures within 10–15 minute intervals along the night, and the continuous lines are the CM measurements. Only one STT point deviates from the CM curve at the end of the night of April 25 (for unclear reasons). Note that June 24 is a night discarded on the CM as the first and last stars were observed inappropriately.

Figure 11 shows the histograms and statistics for those 57 nights when the CM gathered data simultanously with the STT. The median in both cases was 0.58 arcsec and the difference between the respective values of the first quartil is not significant. The shape of the distribution differs slightly for FWHM values larger than 0.7 arcsec. The reason for this is not readily understood but must be related with small number statistics for the STT data and probably also some selection effects related with the selection of *Low xy* measurements.

The agreement between the STT and CM data suggests that our criteria to the selection of STT data
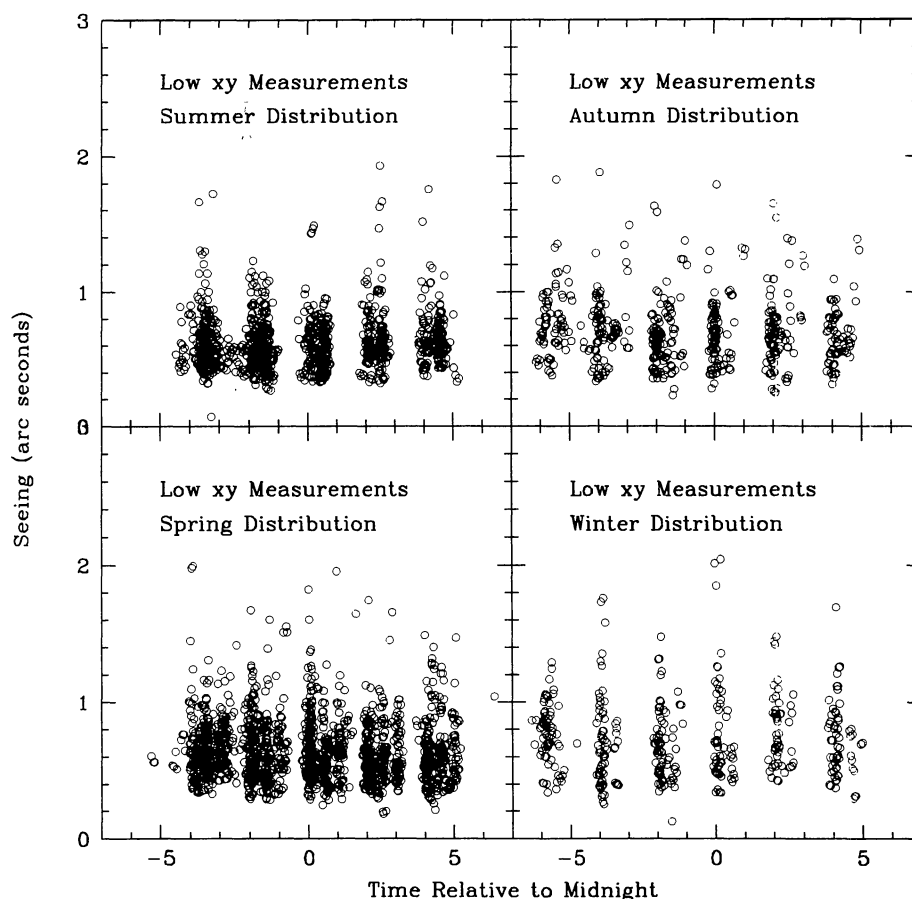

Fig. 21. *Seeing* ver sus night time as a function of season.

unaffected by wind shake are correct and that the difference between a median of 0.69, obtained with the overall y data (see Fig. 6) and a median of 0.61, obtained for the *Low xy* data, is a measurement of the wind vibrations in the y axis.

3.4. *MTA Measurements*

The MTA observations were done during two different periods: from April 16 to May 17 and from June 18 to August 23, 1992. The results are shown in Figure 12. The solid circles correspond to the median of the local *seeing* FWHM image size computed from the median C_T^2 parameters (e.g., Woolf 1982). The local *seeing* is considered to be 0 arcsec at an elevation of 100 m, and it increases as the starlight heads toward the ground and passes through the turbulent boundary layer below 100 m. Above 100 m the image is considered to be degraded by only the turbulent layers of the free atmosphere, which mostly reside at an elevation of 10 km or so.

The total value of the median image size S_T is shown as the upper curve in Figure 12, and given by

$$S_T = (S_L^{5/3} + FA^{5/3})^{3/5} \ ,$$

where S_L is the median local value at the measured height and FA is the *median free atmospheric seeing*, i.e., the image size that one would observe at a height of 100 m, where the local conditions do not affect the quality of the image. The free atmosphere median image size is considered to have a value of $FA = 0.52$ arcsec (Cromwell et al. 1998).

It can be appreciated that the local site conditions do not affect substantially the total value. In fact, if we extrapolate the STT measurements at 3.6 m, then we predict a *free atmospheric seeing* of 0.5 arc-

sec. This implies that at an altitude of 15 m we will have a median of 0.54 arcsec and a first quartil of 0.40 arcsec.

It is important to evaluate the local *seeing* conditions to decide the best altitude for a large telescope. The surface layer contribution (as shown in Figure 12) is important in the first 15 m. Its contribution between 4.2 m and 12 m, and is about 0.21 arcsec, compared with the local *seeing* contribution between 15 m and 28 m which is about 0.12 arcsec. Therefore, we consider this value as the best altitude to put a large telescope at this site.

3.5. *Seeing as a Function of Atmospheric Parameters*

Figure 13 shows the wind velocity-speed distribution in SPM. We have plotted all observations, since these are independent of the criteria to select the *Low* and *High xy* STT data. The graph shows that the wind speed seldom exceeds 40 km s^{-1}. Although the predominant and strongest winds come from the SSW, while the wind rarely comes from the E and WNW, the wind speed distribution appears almost uniform. This is not the case if we separate the data in seasons. Figure 14 shows the wind speed distribution throughout the year. For brevity we have separated the data every three months: January-March; April-June; July-September and October-December, and we have called these quarters winter, spring, summer, and autumm, respectively. Although we have better coverage during spring and summer, it is clear from Figure 14 that the wind distribution has its pecularities at each season. The spring distribution appears uniform, while the summer distribution has a peculiar gap with very few WNW winds. The autumm and winter samples have a bipolar distribu-

TABLE 1

COMPARISON OF *SEEING* RESULTS WITH OTHER SITES

Site	*Seeing*	Instrument	Ref.[a]
Mt. Graham, Arizona, USA	0.60	STT	1
Mt. Hopkins, Arizona, USA	0.59	STT	2
Las Campanas, Chile	0.60	CM	3
La Silla, Chile	0.87	DIMM	4
Paranal, Chile	0.64	DIMM	4
Mauna Kea, Hawaii, USA	0.57	SCIDAR	5
La Palma, Islas Canarias, Spain	0.64	DIMM	6
SPM, B.C., México	0.61	STT, CM	7

[a] References: (1) Cromwell et al. 1998. (2) Cromwell et al. 1990. (3) Persson et al. 1990. (4) Murtagh & Sarazin 1993. (5) Roddier et al. 1990. (6) Muñoz-Tuñón et al. 1997. (7) This paper.

tion, with a rotation of 90° orientation between each other. During the winter the predominant winds come from the NE and SW.

The *seeing Low xy* STT data distribution as a function of wind speed is shown in Figure 15, where we observe a large range of *seeing* values which are independent of the wind speed. Although in general there seems to be no correlation between bad *seeing* and wind speed, there seems to be a slight correlation for good *seeing* values and wind speed. In other words, there is a lower envelope in the graph that precludes good seeing and high wind. In Figure 16 we present the same distribution, but again separated in seasons. The spring and summer distributions are similar to that in the previous figure, but there is very little evidence of a good *seeing* wind speed correlation. However, in the autumn and winter distributions, this correlation is not only much clearer, but there is also an indication of a bad *seeing* wind speed correlation, particularly during the winter months.

The *seeing* as a function of wind direction is shown in Figure 17. Again the distribution appears uniform, while the seasonal distributions, shown in Figure 18 are quite different. The spring and summer distributions reflect their parent distributions shown in Fig. 14, but the autumn and winter samples clearly show that the *seeing* has larger values, particularly when the wind comes from the West during the autumm and from the North in winter.

The *seeing* distribution as a function of season is shown in Figure 19. We confirm here that the *seeing* during the autumn and winter is worse than during spring and summer, with a median difference of about 0.1 arcsec.

Figure 20 shows the *seeing* as a function of time relative to midnight. There is a slight evidence that good *seeing* tends to improve during the night. This might be the case again for the spring sample shown in Figure 21, but not for the other seasons. During the summer, there appears that the good *seeing* might reach an optimal value around midnight, while for autumm and winter the data are not conclusive.

We have also looked at temperature and humidity values as a function of *seeing* (not shown in the figures) and found no substantial correlations. In particular, we found large *seeing* values at low humidity values, but obviously our data are strongly biased in the sense that there are few observations at high humidity, usually associated with clouds.

3.6. *Comparison with other Sites*

A tentative comparison with other observing sites or facilities is made in Table 1. It is tentative, because individual locations on the same mountain have different *seeing* and different profiles through the ground layer. In particular, readers are warned that early measurements suggesting low turbulence

through the tree layer on Mt. Graham from STT that gave a good measurement of telescope *seeing*) are inconsistent with later measurements, which show that the telescope height required for excellent *seeing* there depends on the particular location. Only one location has been measured on SPM, and we do not know how these measures will translate to other locations.

It is of particular importance the comparisons of the STT results here presented with those for Mount Graham and Mount Hopkins, and those obtained with the CM for our site with the results at Las Campanas Observatory; it is possible to compare them directly as they have been measured with exactly the same instruments. We point out that, while the anlysis of the data for Mount Graham and Mount Hopkins is similar to that of SPM, the number of observed nights in our case is much larger. The number of accumulated nights at the reference location (High Peak) in Mount Graham is similar to the number of yearly nights observed at SPM but regrettably, good microthermal measures are not available for the High Peak site, about 2 km from the current High Binocular Telescope (LBT) site observations. Reasonable microthermal measures are available for the LBT site and Mt. Hopkins. The value given in Table 1 for Mt. Hopkins is close to ground level, because the ground layer contribution is very small. For the LBT site, the value given is for an elevation of 30 m, the approximate height of the LBT, and a height where the ground layer contribution is small. Based on these facts we conclude that the *seeing* at SPM is comparable to that of Mount Hopkins. Likewise, the number of nights observed with the Carnegie Monitor is comparable with those observed at Las Campanas Observatory. Since the instrumental setup and reduction methods are identical, again we conclude that the *seeing* at SPM is comparable to that of Las Campanas.

The *seeing* reports for La Silla, Paranal, La Palma, and Mauna Kea are shown in Table 1; they are based on Differential Image Motion Monitors (DIMM), Scintillation Detection, and Ranging (SCIDAR), Sound Detection and Ranging (SODAR) devices, and microthermal sensors. The final values are the convolution of two or more instruments and therefore, cannot be compared straightforwardly. Although our own MTA measurements are comparable with the 10–30 m data for La Silla, their Sodar measurements give a much higher total *seeing* for the latter observatory. In general, our results are similar to those for Paranal and Mauna Kea.

To compare the surface layer or boundary layer contribution with others sites requires observations with the same conditions and equipment, but we can propose some examples: (a) if we interpolate our data to have the surface layer between 6 m and 12 m as in the case of four nights observed at the Ob-

servatorio del Roque de los Muchachos with a mast with detectors at these elevations (Vernin & Muñoz-Tuñón 1994) we obtain 0.15 arcsec compared with the mean value of 0.07 obtained by these authors; (b) we might also compare our results with those of Roddier et al. (1990), for the boundary layer (up to one km) in Mauna Kea and La Silla; our results between 4.2 m and 28 m give a contribution of 0.31 arcsec, compared with 0.28 and 0.73 for Mauna Kea and La Silla respectively; (c) finally we compare our results with those obtained at San Pedro Mártir Observatory by Avila, Vernin, & Cuevas (1998), who observed with a SCIDAR detector at the 2.1-m telescope, and obtained a median *seeing* of 0.45 arcsec above 1 km; 0.58 arcsec within the first kilometer and a median total *seeing* at the 2.1-m telescope of 0.68 arcsec. This last value is consistent with our results since their measurements include the dome *seeing* and therefore should yield a larger value than the open air *seeing* measurements.

4. CONCLUSIONS

A 3 year campaign has been carried out at the site of the Observatorio Astronómico Nacional at San Pedro Mártir to measure the atmospheric turbulence. The results obtained during this period with the Site Testing Telescope yielded a median FWHM *seeing* of 0.61 arcsec and a first quartile of 0.50 arcsec. These values are confirmed by independent measurements with the Carnegie Monitor. There is some seasonal dependence on the *seeing*; we found that the *seeing* is better during spring and summer with a median around 0.59 arcsec compared with 0.69 during autumn and winter. Measurements with the Micro-Thermal Array show that the *seeing* decreases by 0.1 arcsec at a height of 15 meters. The *seeing* does not seem to depend strongly on meteorological variables like wind direction and velocity, humidity or external temperature.

In conclusion the atmospheric turbulence is exceptionally good, comparable with those at Las Campanas, Paranal, Mount Hopkins, La Palma and Mauna Kea sites.

REFERENCES

Alvarez, M. 1982, Reporte Técnico No. 5, Instituto de Astronomía, UNAM

Alvarez, M., & Maisterrena, J. 1977, RevMexAA, 2, 43

Alvarez, M., & Moreno, M. A. 1995, Contribución Interna del Instituto de Astronomía, UNAM, CI-95-01

Avila, R., Vernin, J., & Cuevas, S. 1998, in Interstellar Turbulence, Proceedings of the 2nd Guillermo Haro Conference, ed. J. Franco, A. Carramiñana, (Cambridge: Cambridge Univ. Press)

Cromwell, R.H., Blair, C. N., & Woolf, N. J. 1992, BAAS, 24, 1238

_____. 1998, Site Testing for the High Binocular Telescope, LBT Technical Memo, in preparation

Cromwell, R. H., Haemmerle, V. R., & Woolf, N. J. 1988, in Very High Telescopes and their Instrumentation, ESO Conference Proceedings, ed. M.-H. Ulrich, (Munich: ESO), Vol. II, 917

_____. 1990, SPIE, 1236, 520

Hiriart, D., Goldsmith, P. F., Skrutskie, M. F., & Salas, L. 1997, RevMexAA, 33, 59

Mendoza, E. E. 1971. Bol. Obs. Tonantzintla y Tacubaya, 6, 95

_____. 1973, Mercury, 2, 9

Mendoza, E. E., Luna, J., & Gómez, T. 1972, Bol. Obs. Tonantzintla y Tacubaya, 6, 215

Moreno-Corral, M., Costero, R., & Schuster, W. 1994, Mercury, 23, 29

Muñoz-Tuñón, C., Vernin, J., & Varela, A. M. 1997, A&AS, 125, 183

Murtagh, F., & Sarazin, M. 1993, PASP, 105, 932

Persson, S. E, Carr, D. M., & Jacobs, J. H. 1990, Experimental Astronomy, 1, 195

Roddier, F., et al. 1990, SPIE, 1236, 485

Sarazin, M. 1990, European Southern Observatory, Internal Report, January 1990, (Munich: ESO)

Tapia, M. 1992, RevMexAA, 24, 179

Vernin, J., & Muñoz-Tuñón, C. 1994, A&A, 284, 311

Walker, M. F. 1971, PASP, 83, 401

_____. 1984, in Site Testing for Future High Telescopes, ed. A. Ardeberg & L. Woljer, (Munich: ESO), 3

Westphal, J. A. 1974, Infrared Sky Noise Survey, Final Report NASA-NGR-05-002-185, (Pasadena: Caltech)

Woolf, N. J. 1982, ARA&A, 20, 367

R. Costero and J. Echevarría: Instituto de Astronomía, UNAM, Apartado Postal 70-264, 04510 México, D.F., México (jer@astroscu.unam.mx; costero@astroscu.unam.mx).

O. Harris, Rm. Michel, Rl. Michel, R. Muñoz, J. L. Ochoa, J. Palomares, M. A. Rojas, L. Salas, M. Tapia, and J. Valdez: Instituto de Astronomía, UNAM, Apartado Postal 877, 22800 Ensenada, B.C., México.

R. H. Cromwell and N. J. Woolf: Steward Observatory, University of Arizona, 933 North Cherry Ave., Tucson, AZ 85721-0065, USA.

D. M. Carr and S. E. Persson: The Observatories of the Carnegie Institution of Washington, 813 Santa Barbara St., Pasadena, CA 91101, USA.